Article

Effects of BTEX on the Removal of Acetone in a Coaxial Non-Thermal Plasma Reactor: Role Analysis of the Methyl Group

Liyuan Hou, Xiang Li *, Deyuan Xie and Haining Wang

School of Space and Environment, Beihang University, Beijing 100191, China; houliyuan@126.com (L.H.); xiedeyuan@126.com (D.X.); wanghaining@buaa.com (H.W.)

* Correspondence: xiangli@buaa.edu.cn

Abstract: The removal of acetone and benzene series (BTEX) under individual and concurrent conditions is carried out in a coaxial nonthermal plasma (NTP) reactor. The results show that the benzene series has a significant negative impact on acetone conversion and CO_2 selectivity under NTP treatment. Furthermore, it is found that *p*-xylene significantly promotes CO_x selectivity under co-treatment with acetone because of greater CO generation. Based on the results of transient FTIR, MS, and GC-MS, it is seen that quantities of formic acid, formaldehyde, and ring-opening byproducts from benzene series decomposition are reduced, while quantities of aromatic byproducts with carboxyl, phenolic, and aldehyde groups on the benzene ring increase under coexistence conditions. With the help of theoretical calculation and kinetic analysis, hydrogen abstraction from the methyl group and active hydroxyl radical consumption are proposed as critical factors in the BTEX inhibition effect on acetone degradation.

Keywords: non-thermal plasma; byproducts; methyl group; acetone; BTEX

1. Introduction

As an important predecessor of submicron particles (PM2.5) and ozone pollution in the atmosphere, volatile organic compounds (VOCs) emitted from industrial manufacturing have received increasing attention in recent years [1,2]. Among the VOCs, the benzene series (BTEX) and acetone have always been simultaneously utilized in paints, solvents, and raw materials in the chemical and printing industry [3–5]. Exposure usually causes a number of environment-related health problems, including dizziness, nausea, organ damage, and even cancer [6]. Thus, developing suitable abatement methods for BTEX/acetone emission control is urgent and significant. Conventional technologies for VOC removal include adsorption, thermal combustion, chemical absorption, and catalytic oxidation. However, such methods are not sufficiently cost-effective or suitable for removal of dilute concentrations (<1000 ppm) of contaminants under high space velocity because of low efficiencies and high energy consumption [7]

In recent years, non-thermal plasma (NTP) has been regarded as an energy-saving, efficient, and promising method for low-concentration VOC abatement due to its environmentally-friendly nature, fast ignition response, and strong oxidative degradation ability [8,9]. At room temperature, quantities of highly energetic electrons and reactive species generated in the discharge area trigger a cascade of plasma chemistry reactions, resulting in the removal of pollutants [10–12]. Several studies on BTEX removal, side product analysis, and degradation mechanisms by NTP have been reported over the past few years. Satoh et al. explored the effect of O_2 proportion in carrier gas on the removal of benzene by different manners of discharge. The results shows that at low oxygen concentration,

the byproducts are primarily C_2H_2, HCN, NO, and HCOOH, while only HCOOH is found at high oxygen concentrations [13]. Stefan et al. investigated the degradation of cyclohexene and BTEX in an NTP air purifying system, and the degradation efficiency order of benzene (<1%) < xylene (3%) $\approx$ ethylbenzene < toluene (11%) $\approx$ cyclohexene was found [14]. Our previous research indicates that the conversion of low-concentration benzene, toluene, and *p*-xylene increases from 2%, 19%, and 49%, respectively, at an energy density (ED) of 10 $J \cdot L^{-1}$ under positive corona discharge for BTEX [15]. Unlike BTEX, there are few reports focused on acetone degradation by NTP. In research, monolithic ceramic catalysts and CuO/γ-Al_2O_3 are often added into the plasma reactor or after the reaction to intensify the decomposition of acetone plasma [16,17]. With respect to byproduct investigation, Narengerile et al. evaluated the acetone decomposition efficiency in DC water plasmas at atmospheric pressure. It was found that aqueous acetone can be successfully decomposed into H_2, CO_2, CO, and CH_4, but unwanted byproducts, such as HCOOH and HCHO, also form [18].

However, some limitations on the study of acetone and BTEX removal by NTP still exist as follows. Firstly, acetone, as a representative of oxygen-containing VOCs, is hardly decomposed, but has the highest emission limit (100 $mg \cdot m^{-3}$) among VOCs from petrochemical industry emissions [19]. However, few studies have focused on its removal effectiveness, especially at low concentrations. Secondly, in general typical industrial emissions contain a blend of VOCs [20,21]. However, research often focuses on single-component VOCs rather than mixtures of VOCs, which is not in accordance with real emission conditions. Thirdly, though BTEX concentrations are far below those of acetone in real life, their compounds are characteristic constituents of the gaseous effluents of wastewater treatments in petrochemical plants [19]. Whether there is an interaction between acetone and BTEX when treated together remains unknown.

Accordingly, this study focuses on a mixture of acetone and BTEX degradation using corona discharge that aims at investigating possible influencing mechanisms in removal efficiency and COx selectivity under NTP treatment. In addition, the impact of BTEX types on NO_x, O_3, organic byproduct formation, and the acetone degradation pathway are also studied by experimental and theory calculations in this paper.

2. Experimental

2.1. Experimental System

The experimental system is shown in Figure 1. It consists of a coaxial link tooth wheel-cylinder plasma reactor with a 25 kV/5 mA negative direct current (DC) high voltage power supply, reaction gas supply, and analytical instrumentation. It is a stainless steel cylinder with an inner diameter of 42 mm and a length of 300 mm that serves as the ground electrode of the plasma reactor. The high voltage electrode is a stainless steel rod (o.d. 6 mm) through which 10 discharge teeth wheels are linked with a space interval of 10 mm, while each wheel has six discharge cusps. The effective discharge length and discharge intervals are 100 and 16 mm, respectively. The visual appearance of the discharge is that of a gleamy plasma column completely filling the inter-electrode space, representing a streamer-like corona discharge.
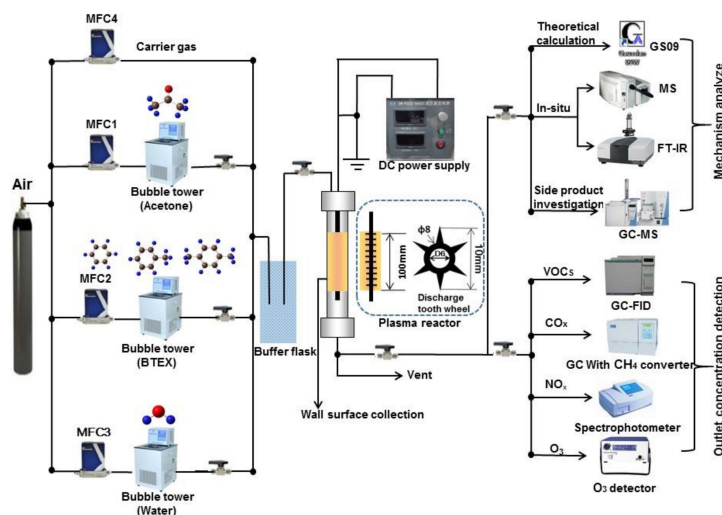
Figure 1. Schematic diagram of the experimental system.

2.2. Experimental Methods

Experiments with both the single acetone and acetone with BTEX (benzene, toluene, or *p*-xylene) were conducted in this study. Gaseous VOCs and water vapor were introduced by passing air through a temperature-controlled bubble tower and they were then mixed with dilution air in a mixing chamber to reach the desired concentration. Relative humidity (RH) of the reaction gas was controlled at 50% at room temperature (298 K). The concentrations of benzene, toluene and *p*-xylene were all 50 ppm, while that of acetone was 250 ppm. The total flow rate was 2.0 L·min^{-1}. All the reagents used in this study were analytically pure, obtained from the Beijing Chemical Corporation (Beijing, China).

The outlet concentrations of the VOCs, CO_x (CO and CO_2), O_3, NO_x (NO and NO_2) were respectively detected. The VOCs in the gas stream were analyzed by an online gas chromatograph (Agilent, model 6890N, Santa Clara, CA, USA), equipped with a flame ionization detector (FID) and a 30.0 m × 320 μm HP-5 capillary column. The column temperature was 373 K and that of the detector was 423 K. The conversion of each VOC by non-thermal plasma (NTP) decomposition was defined by η, calculated according to Equation (1). The energy density (ED, J·L^{-1}) was used to evaluate the validity of NTP technology, which was calculated according to Equation (2). In the present work, all the decomposition results were compared and discussed based on the ED. The outlet concentrations of CO and CO_2 were analyzed by a gas chromatograph (Techcomp, model GC7890II, Beijing, China) equipped with an FID detector, a TDX-01 packed column, and a methane conversion oven prior to the detector. The CO_x selectivity was adopted to characterize the mineralization degrees of the VOCs in the present work, defined by SCO_x according to Equation (3). O_3 was monitored by the Ozone Monitor (2B Technologies, 106-L, Boulder, CO, USA) according to the ultraviolet absorption method, while NO_x was monitored according to the *N*-(1-naphthyl) ethylene diamine dihydrochloride spectrophotometric method.

$$\eta = \frac{C_{inlet} - C_{outlet}}{C_{inlet}} \times 100\%, \tag{1}$$

$$ED = \frac{U \times I}{Q} \times 60 \tag{2}$$

$$S_{CO_x} = \frac{(2-x)C_{CO} + (x-1)C_{CO_2}}{\sum n_{inlet}C'_{inlet}\eta} \times 100\% \tag{3}$$

where C_{inlet} and C_{outlet} are inlet and outlet concentrations of the pollutant (ppm), respectively; *U* and *I* are the applied voltage (kV) and discharge current (mA), respectively, both of which can be automatically detected by the power supply equipment, checked before experiments; and *Q* is the flow rate of the

reaction gas (L·min^{-1}). C'_{inlet} is the inlet concentration of the pollutant (mg·m^{-3}); CCO$_2$ and CCO are the outlet concentrations of CO$_2$ and CO (mg·m^{-3}); and ninlet indicates the number of carbon atoms of the VOC.

2.3. Characterization

In order to clarify the mechanism of VOC degradation by NTP, the variations in the intermediate products were detected by a mass spectrometer (MS OmnistarTM, model GSD 301 O2, Preddvor, Slovenia) and Fourier transform infrared spectroscopy (FTIR, Nicolet 6700, Santa Monica, CA, USA). The mass spectrometer was used to explore the change of intermediate species during the reaction process. An electron multiplier and a tungsten filament were used to detect the specific charge, while the SEM voltage was controlled at 1.4 kV. The first mass was 44.5 u and the last mass was 100 u, except for *p*-xylene (110 u). The scan speed was 5 s. FTIR was used to investigate the change of the gas molecule functional group during the reaction process; all spectra were collected in the 3700–600 cm^{-1} frequency range at a resolution of 4 cm^{-1}. In total, 16 scans were averaged for each spectrum, while the gathering time was 20 min.

The organic side products were collected using 5 mL methyl alcohol for 15 min, and then identified using gas chromatography–mass spectrometry (GC–MS, Shimadzu GC-2020, Kyoto, Japan) in electron impact mode (70 eV), equipped with a 60.0 m × 0.25 mm × 0.25 μm column (Agilent, HP5MS, Santa Clara, CA, USA), A 200 °C ion source was chosen. Argon was chose as the carrier gas and the flow rate was 1 mL·min^{-1}.

The theory calculation was based on the Gaussian 09 package program combined with density functional theory (DFT). The molecular geometry of the VOCs was optimized using the DFT (B3LYP) method with a 6-311G++(d,p) basis set. The atomic partial charge, bond length, and electrostatic potential of HOMO orbits of the VOCs were calculated, and the corresponding results are listed in Table S1.

3. Results and Discussion

3.1. Effect of BTEX on the Acetone Removal Efficiency

Acetone and BTEX conversions are studied as a function of energy density under the conditions of individual contaminants and two VOC mixtures. As shown in Figure 2a, when acetone is treated individually, its conversion increases from 0% to 71% with increasing ED. This result is similar to that of a previous study by Zheng et al. [22]. However, when acetone is degraded together with three kinds of BTEX under plasma treatment, its degradation efficiency reduces to less than 20% with an energy density of 1200 J·L^{-1}, implying that BTEX has a significant negative impact on acetone conversion. The degree of influence of three different kinds of BTEX on acetone removal efficiency can be ordered as follows: toluene ≈ *p*-xylene > benzene.

However, it can be seen from Figure 2b that benzene conversion is hardly affected when it coexists with acetone, while the removal efficiencies of toluene and *p*-xylene decrease with the introduction of acetone. In addition, it is found that whether treated together with acetone or not, *p*-xylene conversion is much higher than that of toluene under the same ED. It is known that high-energy electrons ranging from 1011 to 1014 cm^{-3} contribute to VOC decomposition during the NTP process by two means: (1) directly breaking VOC molecules into organic fragments via high-speed collision; and (2) interaction with carrier gas molecules to generate large quantities of chemical reactive species (e.g., •O, •OH, O$_3$, and metastable N$_2$) for VOC removal [23]. On one hand, the original concentration of BTEX (50 ppm) in this study is far lower than that of acetone (250 ppm), and thus the probability of effective electron collision with acetone molecules may not change significantly after BTEX introduction. In other words, the types and concentration levels of active radicals in the NTP reactor should play a dominant role in contributing to BTEX inhibiting acetone degradation. On the other hand, the structural difference between the three kinds of VOCs is shown in the methyl group and its quantity in the

benzene. Considering the efficiency difference shown in Figure 2, besides the benzene ring effect, it can be deduced that the hydrogen abstraction reactions on the methyl group may occur during BTEX degradation, also influencing the acetone plasma–chemical reactions, removal efficiency, and the degradation product.
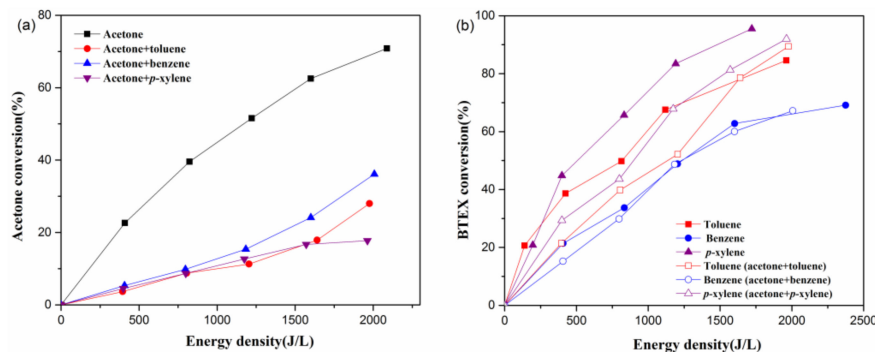

Figure 2. Effects of energy density on acetone (**a**) and BTEX conversion (**b**). Reaction conditions: acetone: 250 ppm, BTEX: 50 ppm, relative humidity (RH): 50%, and total flow: 2 L/min.

3.2. Effect of the BTEX on CO_x Selectivity

Figure 3 shows the selectivity of CO_x as function of ED for the NTP process. It can be seen that in the case of BTEX and acetone together, the CO_x yield shows two stark divergences of trends: addition of *p*-xylene significantly promotes CO_x selectivity, thereby improving acetone mineralization; while CO_x production decreases after adding benzene or toluene into the NTP reaction system, meaning that more organic intermediates form. Figures S1 and S2 also provide the CO and CO_2 selectivity under the binary and single-component VOC degradation processes. It is shown that more CO is generated when methylic BTEX and acetone are treated together, but the tendency is reversed for benzene introduction. By contrast, the selectivity of CO_2 in the binary VOC degradation process is obviously lower than in single-component VOCs. Because more active free radicals are consumed when BTEX is treated together with acetone, the rate of CO_x mineralization and further oxidation of CO to CO_2 is restricted. Equally important is that the hydrogen abstraction reaction on the methyl group occurred more easily with toluene or *p*-xylene degradation, which can lead to CO formation despite an adversity to the total oxidation of pollutants [24,25].
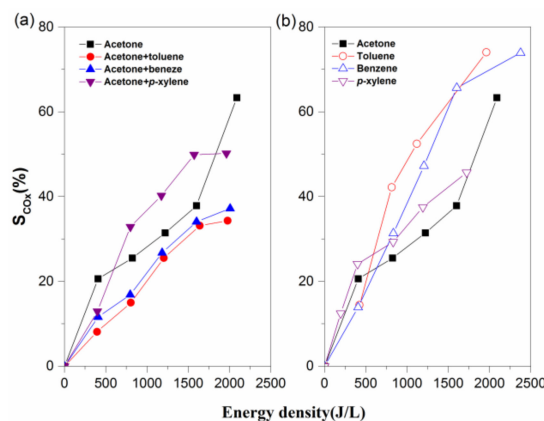

Figure 3. Effects of energy density on the Sco_x of the binary (**a**) and single-component (**b**) volatile organic compound (VOC) degradation processes. Reaction conditions: acetone: 250 ppm, BTEX: 50 ppm, RH: 50%, and total flow: 2 L/min.

3.3. NO$_2$ and O$_3$ Formation Analysis

Figures 4 and 5 provide the relationships between NO$_2$, O$_3$ concentrations and ED. As shown in the two figures, NO$_2$ and O$_3$ production monotonically increases with the increase of ED under both single and binary VOC mixture sets. Notably, the maximum NO$_2$ concentration is less than 1 ppm, and NO is hardly detected in this study, so the effect of BTEX adding on NO$_x$ formation may be negligible. It believed that O$_3$ concentration is greater in the absence of VOCs at a relatively high ED (>200 J·L^{-1}) considering ozone consumption by the oxidation of VOCs [26,27]. Therefore, even though VOC mixture degradation under the NTP process follows complex mechanisms, there may be some correlations between the ozone concentrations and pollutant treatment efficiency. Figure 6 gives the effect of O$_3$ concentration on VOC concentrations. It can be seen that each BTEX conversion enhances significantly with increasing ED when degraded simultaneously with acetone, while acetone follows an inverse pattern. This phenomenon can be explained by the fact that BTEX oxidizes faster than acetone, since the former has a higher reaction rate constant with O$_3$ and •OH [28]. Furthermore, there is significant positive linear correlation between O$_3$ concentration and *p*-xylene conversion, while it is poor for other VOCs. Combined with the lowest yield of O$_3$ for xylene-containing atmosphere degradation (Figure 5), it is reasonable to infer that O$_3$ or its precursor from the plasma–chemical reactions can interact with the methyl group from the *p*-xylene molecule.
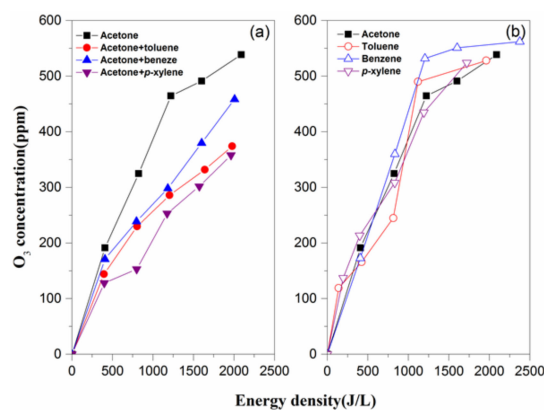

Figure 4. Effects of energy density on the O$_3$ concentrations of the binary (**a**) and single-component (**b**) VOC degradation processes. Reaction conditions: acetone: 250 ppm, BTEX: 50 ppm, RH: 50%, and total flow: 2 L/min.
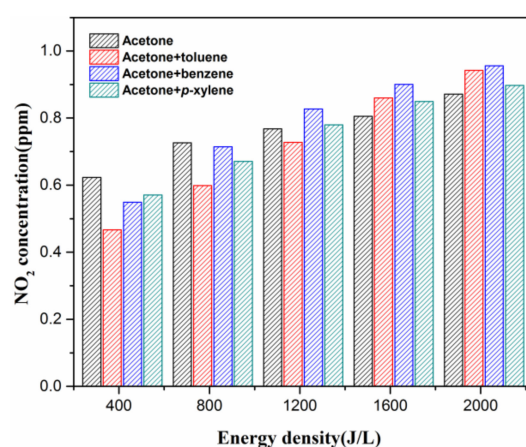

Figure 5. Effects of energy density on NO$_2$ production. Reaction conditions: acetone: 250 ppm, BTEX: 50 ppm, RH: 50%, and total flow 2 L/min.
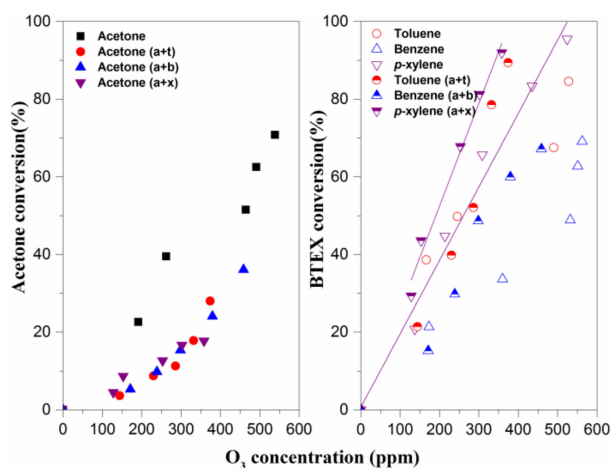
Figure 6. Effects of the O_3 concentrations on acetone (**left**) and BTEX (**right**) conversions. Reaction conditions: acetone: 250 ppm, BTEX: 50 ppm, RH: 50% and total flow 2 L/min.

3.4. Transient Study during NTP Treatment

Figure 7 and Table S1 show the detailed in situ FT-IR spectra of the acetone and acetone–BTEX mixture effluents under plasma treatment at an ED of 1600 $J \cdot L^{-1}$. When acetone is degraded alone, as the reaction time extends the bands at 1027 and 1054 cm^{-1}, ascribed to the O-O stretching vibrations of the ozone, gradually increase. Besides, bands appear at 2126, 2096, 1731, 1441, 1373, 1343, 1302, 1210, 1161, 1121, 1093, and 885 cm^{-1} during the NTP process. Among them, the acetone species are characterized by the ν (C=O) at 1731 cm^{-1}, δ (CH_3) at 1441–1371 cm^{-1} and δ (C-C) at 1161 cm^{-1} [29,30]. As the reaction time continues, the intensity of the bands attributed to olefins (885 cm^{-1}), formic acid (1093 and 1121 cm^{-1}), oxalic acid (1302 cm^{-1}), alcohol (1343 cm^{-1}), and CO (2126 and 2096 cm^{-1}) continuously increases on the spectra [16,31,32]. Narengerile's research results indicate that HCOOH, HCHO, and soot are the main organic byproducts when acetone is decomposed by direct current (DC) plasma [18]. Therefore, the bands belong to the ν (C=O) stretching vibration of the aldehydes, which is usually located at around 1700 cm^{-1}, and may be covered by the characteristic peak of acetone at 1730 cm^{-1}.
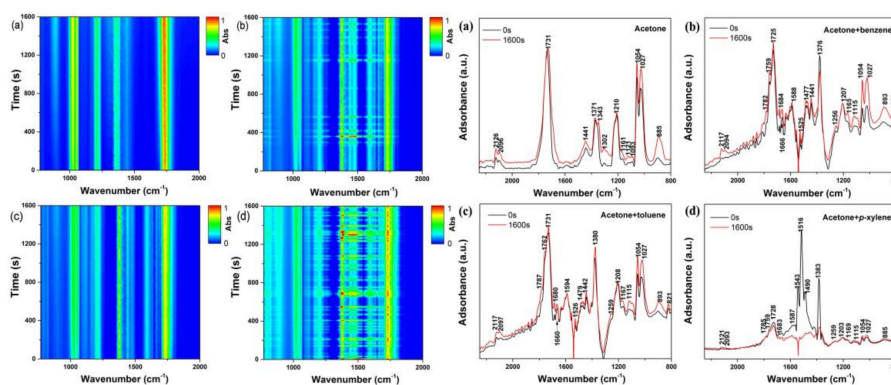

Figure 7. In situ FTIR results of the VOC degradation process at energy density (ED) = 1600 J/L: acetone (**a**); acetone–benzene (**b**); acetone–toluene (**c**); acetone–*p*-xylene (**d**).

For the two composite VOC atmospheres, the FTIR spectra in the range of 1800–1000 cm^{-1} are significantly different from those of the acetone system. The bands at 821 cm^{-1}, 1475 cm^{-1}, 1516–1526 cm^{-1}, and 1660–1684 cm^{-1} represent the characteristic vibrational peaks of the benzene ring. The byproducts related to BTEX degradation consist of the phenolic hydroxyl (OH, 1252–1258 cm^{-1}), aldehyde (CHO, 1759 cm^{-1}), and carboxyl (COOH, 1787 cm^{-1}) group, indicating that phenol, benzaldehyde,

and benzoic acid may form under NTP treatment [33]. In the case of the acetone–xylene composite, the signal-to-noise ratio is significantly lower than for the acetone–benzene and acetone–toluene systems, meaning *p*-xylene becomes extremely unstable under the discharge condition. Additionally, the characteristic peaks of *p*-xylene at 1516 cm^{-1} disappear rapidly after treatment with NTP, suggesting its reaction rate is faster than for benzene and toluene. As shown in the Figure 7, production of O_3 is greater as the reaction progresses, while the reverse result is found when benzene or toluene is treated alone (Figure S3). In general, ozone generated by NTP can be partly consumed by the oxidation of VOCs, but this is suppressed when acetone and BTEX coexist [27]. One possible explanation is that a harder degradation of acetone inhibits the reaction between BTEX and ozone, thereby augmenting O_3 concentrations.

Figure 8 shows the in situ MS spectrum of VOCs degradation at various discharge times. It is obvious that the production of *m/z* 45, 46, 58, 78, 91, and 106 occurs during NTP treatment. Among these, *m/z* 58, 78, 91, and 106 can be mostly attributed to acetone, benzene, toluene, and *p*-xylene, while *m/z* 45 and 46 can be attributed to the oxalic acid or fragment of carboxyl and formic acid, respectively. From this finding, together with the FTIR results, it can be speculated that a hydrogen abstraction from the benzene ring leads to a phenyl radical formation, which would react with ●OH to form benzaldehyde and phenol or be further oxidized to benzoic acid. According to previous research, the hydrogen abstraction reaction from the methyl group will inevitably occur when toluene and acetone are decomposed by NTP and sequentially a reaction occurs with the excited ●OH to form HCOOH, HCHO, and Cox [16,25]. It is reasonable to infer the proportion of formic acid in the carboxylic acid byproduct by the peak area ratio of *m/z* 46 to 45. When BTEX and acetone are treated together, the proportion of formic acid is clearly reduced compared with acetone alone, indicating that the acetone decomposition pathway is influenced by BTEX. Moreover, Figure 8 also gives the acetone degradation rate under different atmospheric conditions. It is clear that the benzene and toluene slightly accelerate the acetone removal but *p*-xylene lessens it. As is well known, benzene can be directly oxidized to various ring-opening byproducts under NTP, while for toluene or xylene, substituent groups on the benzene are more susceptible to decomposition, and benzene series byproduct generation occurs easily [15,34]. Therefore, more methyl group fragments derived from *p*-xylene or toluene decomposition may inhibit the acetone removal, which can also be decomposed to the methyl group and other products under NTP.
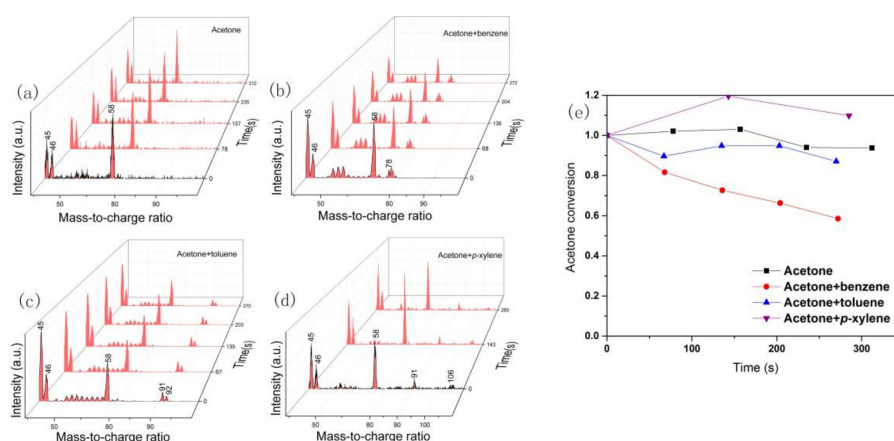

Figure 8. In situ mass spectrometry result of the outlet gas at ED = 1600 J/L: Acetone (**a**), acetone and benzene (**b**), acetone toluene (**c**) and acetone and *p*-xylene degradation (**d**) and acetone conversion (**e**).

3.5. Organic Product Analysis by GC-MS

The organic byproducts of the effluent gas at ED of 1600 J·L^{-1} for single and binary VOCs systems are collected by GC-MS, as shown in Figure 9. The main byproducts during acetone degradation are annular and long-chain oxy-organics containing aldehyde, ethers, esters, etc. The number of organic byproducts, including both aromatic and ring-opening byproducts generated for benzene removal, is significantly greater than for toluene and *p*-xylene. Furthermore, it is seen that ring-opening

byproducts show a significant decrease with the amount of methyl groups on the benzene ring. The major byproducts in the effluent gas of *p*-xylene treatment are benzene, toluene, 4-methyl benzaldehyde, 4-methylbenzoic acid, and benzyl methyl ether. When acetone and BTEX are treated together, the number of light ring-opening byproducts like dimethyl oxalate, methyl dimethoxyacetate, and dimethyl maleate is reduced, while the number of byproducts with more substituent groups on the benzene ring such as o-tolualdehyde, o-nitrophenol, and *p*-toluic acid rises. This phenomenon implies that instead of BTEX ring-opening, methylation and electrophilic substitution reactions in the benzene ring are favored under *co*-treatment of acetone and BTEX by NTP. Therefore, it can be concluded that the methyl group on acetone, toluene, and *p*-xylene decomposing into methyl fragments or radicals may have an immediate impact on the byproduct formation through a series of plasma chemical reactions.
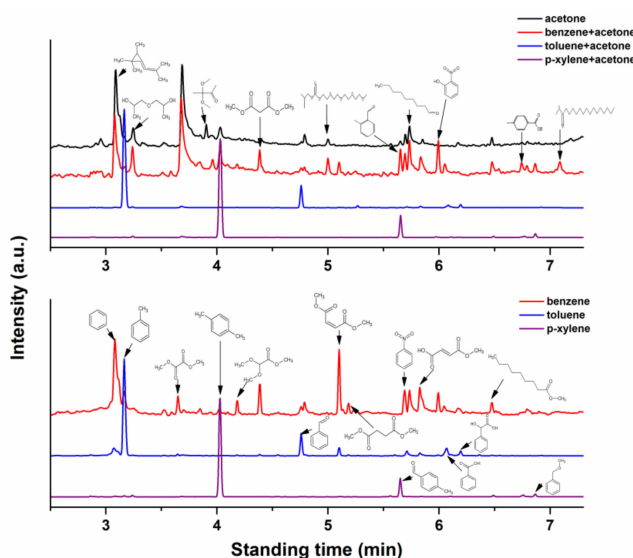

Figure 9. GC-MS results of the outlet gas at ED = 1600 J/L.

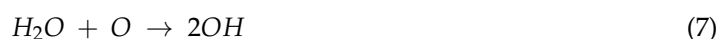### 3.6. Theoretical Analysis of Intermediates

In order to explore the mechanisms of the influence of BTEX on acetone decomposition, acetone and BTEX molecules underwent geometry optimization using the Gaussian 09 package program. Since VOCs are attacked by highly active oxygen species like ●OH and ●O through the electrophilic reactions, the attack position of active radicals on pollutants should have the greatest electron density in the HOMO orbital of the molecule, in accordance with the "frontier orbital" theory [35,36]. Therefore, the bond length, atomic charge, and electrostatic surface potential of total density and HOMO orbitals of the VOCs molecules are also calculated by the density functional theory, as shown in Figure S4 and Table S1. As seen in Figure S3, the positive electrostatic potential of acetone molecule is mainly concentrated in the region around the C1 and C3 atoms, whose atomic charge is −0.763 e on has the strongest electronegativity. Meanwhile, the C1–C2 bonds have the longest bond length (1.517 Å), so the cleavage of the methyl group would be the easiest step during the acetone decomposition process.

According to the ESP of HOMO orbitals for BTEX, it is found that introducing electron-donating methyl groups enhances the electron density of the benzene ring, facilitating attack by free radicals. Therefore, the substituent group position on the benzene ring would be easily occupied by electrophilic ●OH radicals, resulting in further aromatic byproduct formation. On the other hand, as listed in Table S1, the carbon–carbon bond length on the benzene ring is shorter than that between the benzene ring and the substituent group. Thus, *p*-xylene with more methyl groups is more easily substituted through electrophilic reactions than other types of BTEX. Considering the higher electron density
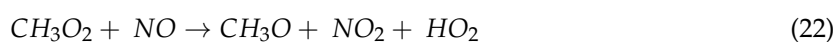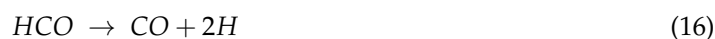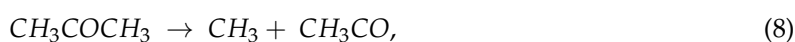
on the benzene ring, greater energy should be provided for ring-opening, thereby inhibiting the non-aromatic hydrocarbon byproducts, which may be a reasonable explanation for the GC-MS result. Consequently, after the –CH$_3$ on toluene and *p*-xylene is removed from the aromatic ring, intermediates such as phenol, benzaldehyde, and benzoic acid would be generated. At the same time, the falling methyl fragment would have a negative impact on acetone decomposition because it may lead to broken acetone regeneration.

3.7. BTEX Effect on Acetone Degradation Pathway

The decomposition mechanism of acetone under various plasma treatment conditions has been reported and discussed by previous researchers [16–18,30]. The relative reaction rate constants involved are summarized in Table S2. When humidity is introduced into the reactor, the main reactive species are oxygen and hydroxyl radicals because O$_3$ can act as a source of their formation, in accordance with Reactions (4)–(7) [37]:

$$N_2 \ + \ O_2 \ + hv \rightarrow \ N_2 + \ 2O, \tag{4}$$

$$H_2O \ + \ hv \rightarrow \ H + \ OH \tag{5}$$

$$O_3 \ + \ hv \rightarrow \ O_2 + \ O \tag{6}$$

$$H_2O \ + \ O \ \rightarrow \ 2OH \tag{7}$$

High-energy electrons •OH and N$_2$* directly dissociate acetone molecules into the fragment of •CH$_3$ and CH$_3$CO• via Reaction (8). Subsequently, the recombination of •CH$_3$ and the oxygen species via several steps (Reactions (9)–(13)) can form CH$_3$O$_2$•, CH$_3$O• and HCHO. The latter is further oxidized to HCO• by •OH or divided into CO and H (Reactions (14) and (15)) [38]. Additionally, HCO• is also the precursor of the CO and CO$_2$, according to Reactions (16–19). Besides, a trace of NO$_2$ can be detected, which may follow Reactions (20)–(23) [39].

$$CH_3COCH_3 \ \rightarrow \ CH_3 + \ CH_3CO, \tag{8}$$

$$CH_3CO \ + \ O \ \rightarrow \ CH_3 + CO_2 \tag{9}$$

$$CH_3 \ + \ O_2 \ \rightarrow \ CH_3O_2 \tag{10}$$

$$CH_3 \ + \ O_3 \ \rightarrow \ CH_3O \ + \ O_2 \tag{11}$$

$$CH_3 \ + \ O \ \rightarrow \ HCHO \ + \ H \tag{12}$$

$$CH_3O + \ O_2 \ \rightarrow \ HCHO \ + \ OH \tag{13}$$

$$HCHO \ + \ OH \ \rightarrow \ HCO \ + \ H_2O \tag{14}$$

$$HCHO \ \rightarrow \ 2H + \ CO \tag{15}$$

$$HCO \ \rightarrow \ CO + 2H \tag{16}$$

$$HCO \ + \ O \ \rightarrow \ CO + \ OH \tag{17}$$

$$CO + \ O \ \rightarrow \ CO_2 \tag{18}$$

$$CO + \ OH \ \rightarrow \ CO_2 + HO_2 \tag{19}$$

$$N_2 \ \rightarrow 2N \tag{20}$$

$$N \ + \ O_3 \rightarrow \ NO + \ O \tag{21}$$

$$CH_3O_2 + \ NO \rightarrow CH_3O + \ NO_2 + \ HO_2 \tag{22}$$

$$NO + \ O \rightarrow NO_2 \tag{23}$$

On the basis of previous results, hydrogen abstraction, ring-opening, and isomerization are the major possible chemical pathways for BTEX oxidation by non-thermal plasma [11,15,40]. Nevertheless, each degradation pathway depends on the oxygen or hydroxyl radicals, and hence the acetone degradation is unavoidably influenced by BTEX because of radical consumption. On the one hand, in the light of a semi-empirical first-order kinetic model provided by previous studies, the reaction rate constant with O for the removal of *VOCs* in the NTP reactors can be predicted using Reactions (24) and (25) when the *VOC* removal is below 95% [26,41].

$$O + [VOCs] \xrightarrow{k} products, \tag{24}$$

$$\frac{[VOCs]}{[VOCs]_0} = e^{-ED/\beta} \tag{25}$$

where k, $[VOC]_0$, and β are represent the reaction rate constant, original concentration of the VOC, and the regression parameter that is equal to $-1/k$, respectively. The k values calculated by different VOC atmospheres as a function of the hydrogen weight fraction are shown in Figure 10 and Table S3, because dehydrogenation reaction by O tends to be carried out on the methyl groups of VOCs undergoing treatment. The result shows that the order of BTEX reactivity is as follows: *p*-xylene > toluene > benzene, in agreement with the descending order of the methyl group amount. Furthermore, its impact trend on acetone reactivity implies that a greater hydrogen fraction in BTEX generally results in a greater loss of the acetone rate constant. On the other hand, since other possible pathways of VOC degradation may include ion–molecule, electrophilic and hydroxyl radical, and ozone reactions, ionization energy, proton affinity, and reaction constants (298 K) with the ●OH and O_3 of pollutants are referred to from the NIST and listed in Table 1 [42]. It is found that ozone reactivity is negligible, since reaction rate constants for ozone are far lower than for the hydroxyl radical. Both the sequence of ●OH reaction constants and ease of ionization follow the (decreasing) order *p*-xylene > toluene > benzene > acetone, in consensus with the O reaction rate mentioned above. Thus, it is suggested that BTEX may be decomposed firstly rather than acetone. However, the order of proton affinities is as follows: acetone > *p*-xylene > toluene > benzene, implying acetone is chemically more reactive with electrophilic reagent than BTEX. It thus stands to reason that acetone can react with electrophilic intermediate species generated from hydrogen abstraction reaction on the methyl group under BTEX decomposition, thereby changing the original degradation pathway.
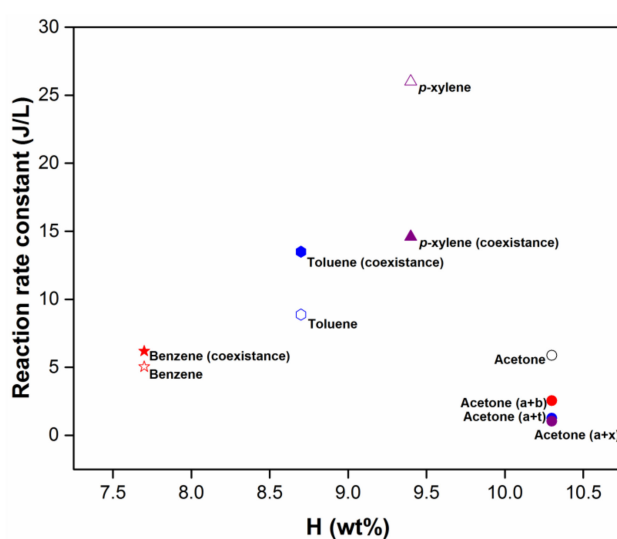

**Figure 10.** Reaction rate constants of the VOCs with O vs. the hydrogen weight fraction H (wt %).

Table 1. The values for ionization energies, proton affinities, and reaction constants for reactions with the •OH and O_3 of VOCs.

VOCs	IE (eV)	PA (kJ/mol)	k_{OH} (cm^3 molecule^{-1}s^{-1})	k_{O3} (cm^3 molecule^{-1}s^{-1})
Acetone	9.70	812.0	3.90×10^{-14}	nf
Benzene	9.24	750.4	1.28×10^{-12}	1.72×10^{-22}
Toluene	8.83	784.0	6.16×10^{-12}	3.9×10^{-22}
p-xylene	8.44	794.4	1.52×10^{-11}	nf

nf—not found in the NIST.

3.8. Roles of Methyl Species in the Acetone Degradation

In the plasma environment, acetone can be firstly decomposed into CH_3• and CH_3CO• by active radicals and high-energy electrons, as mentioned above (Equation (9)). Then, these two intermediates further go through a series of oxidation reactions to generate CO, CO_2 and other byproducts by collisions with O or •OH radicals. As is well known, the methyl group ($-CH_3$) usually plays a key role in the C1 chemistry, because it is the main precursor of HCHO, HCOOH, and other organic micro-molecules [43]. Therefore, it is believed that the fate of the hydrogen abstraction reaction on the methyl group largely determines the oxidation regime of acetone, as pointed by Alzueta's research [24]. When acetone is treated together with methylic BTEX, amounts of intermediate products from methyl group reaction are inevitably generated and further participate in acetone degradation. For Reaction (9), there is an unfavorable shift in the equilibrium through the increase in the products, resulting in the decreased degradation efficiency of acetone, as well as that of toluene and *p*-xylene. This may be also a reasonable explanation for the immunity effect of benzene shown in Figure 2. Furthermore, considering a limited number of active radicals (mainly •OH), amounts of CH_3• from acetone degradation would react with CO rather than being completely oxidized to CO_2, leading to CO_2 selectivity decreasing. Finally, the methyl group with electron-donating effect can promote the electron density of the benzene ring, which makes electrophilic •OH more easily consumed on the benzene ring than acetone, thereby intensifying aromatic byproduct formation. Therefore, a summary schematic diagram of the influencing mechanism of BTEX on the acetone degradation pathway is proposed, as shown in Figure 11.
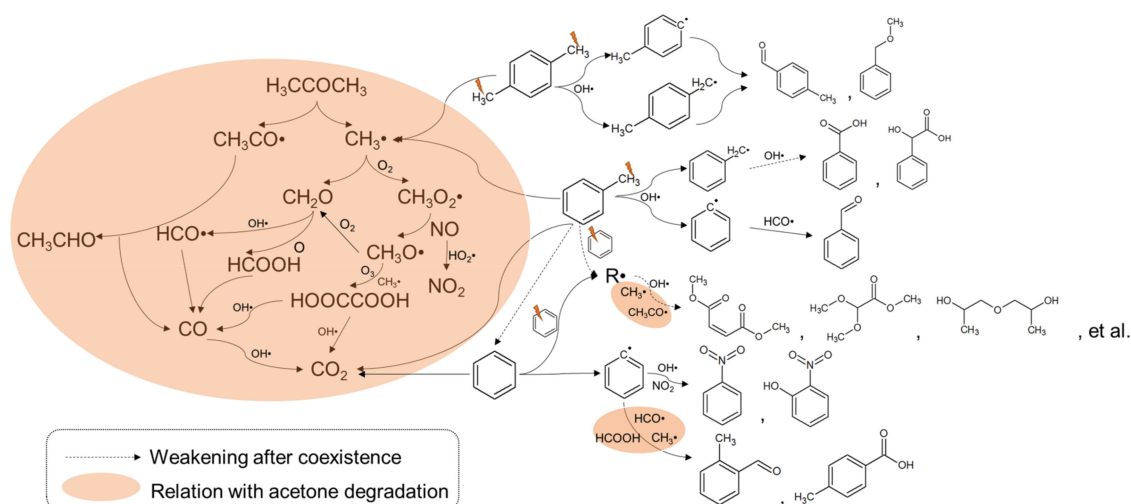
Figure 11. Schematic diagram of the influence mechanism of BTEX on the acetone degradation pathway.

4. Conclusions

In this research, the effect of BTEX on acetone degradation by non-thermal plasma was investigated in depth under negative DC corona discharge in humid air. The primary findings are as follows:

(1) BTEX has a significant negative impact on acetone conversion when they are treated together. The degree of influence of the three different kinds of BTEX on acetone removal efficiency can be ordered as follows: toluene ≈ *p*-xylene > benzene.

(2) *p*-xylene significantly promotes CO generation, thereby improving CO_x selectivity; while benzene or toluene decreases CO_x selectivity after coexistence with acetone.

(3) Based on the results of in situ experiments and GC-MS, it is found that the quantity of ring-opening byproducts is reduced, while the number of aromatic byproducts rises under abatement of mixture VOCs, indicating that instead of BTEX ring-opening, methylation, and electrophilic substitution reactions in the benzene ring are favored during decomposition.

(4) It is deduced that methyl radicals play an important inhibiting role in degradation efficiency and CO_x selectivity, which is mainly shown through: (1) unfavorable shifting of the equilibrium of acetone degradation reaction through the increase in the products; (2) reaction with limited active radicals to generate CO rather than highly oxygenated CO_2; and (3) intensified side reactions on the benzene ring, thereby promoting aromatic byproduct formation.

Author Contributions: L.H. and X.L. conceived and designed the experiments; L.H. and D.X. performed the experiments; L.H. and X.L. analyzed the data; L.H., D.X. and H.W. contributed reagents/materials/analysis tools; L.H. and X.L. wrote the paper.

Conflicts of Interest: The authors declare no conflict of interest.

References

1. Gong, X.; Kaulfus, A.; Nair, U.; Jaffe, D.A. Quantifying O_3 impacts in urban areas due to wildfires using a generalized additive model. *Environ. Sci. Technol.* **2017**, *51*, 13216–13223. [CrossRef] [PubMed]

2. Liao, K.J.; Tagaris, E.; Napelenok, S.L.; Manomaiphiboon, K.; Woo, J.-H.; Amar, P.; He, S.; Russell, A.G. Current and future linked responses of ozone and PM2.5 to emission controls. *Environ. Sci. Technol.* **2008**, *42*, 4670–4675. [CrossRef] [PubMed]

3. Chen, W.-H.; Chen, Z.-B.; Yuan, C.-S.; Hung, C.-H.; Ning, S.-K. Investigating the differences between receptor and dispersion modeling for concentration prediction and health risk assessment of volatile organic compounds from petrochemical industrial complexes. *J. Environ. Manag.* **2016**, *166*, 440–449. [CrossRef] [PubMed]

4. Jiang, L.; Zhu, R.; Mao, Y.; Chen, J.; Zhang, L. Conversion characteristics and production evaluation of styrene/o-xylene mixtures removed by DBD pretreatment. *Int. J. Environ. Res. Public Health* **2015**, *12*, 1334–1350. [CrossRef] [PubMed]

5. Ushiki, I.; Sato, Y.; Ota, M.; Inomata, H. Multicomponent (binary and ternary) adsorption equilibria of volatile organic compounds (acetone, toluene, and n-hexane) on activated carbon in supercritical carbon dioxide. *Ind. Eng. Chem. Res.* **2016**, *55*, 2163–2173. [CrossRef]

6. Vandenbroucke, A.M.; Mora, M.; Jimenez-Sanchidrian, C.; Romero-Salguero, F.J.; De Geyter, N.; Leys, C.; Morent, R. TCE abatement with a plasma-catalytic combined system using MnO$_2$ as catalyst. *Appl. Catal. B* **2014**, *156*, 94–100. [CrossRef]

7. Karuppiah, J.; Reddy, E.L.; Reddy, P.M.; Ramaraju, B.; Karvembu, R.; Subrahmanyam, C. Abatement of mixture of volatile organic compounds (VOCs) in a catalytic non-thermal plasma reactor. *J. Hazard. Mater.* **2012**, *237–238*, 283–289. [CrossRef] [PubMed]

8. Wang, W.; Fan, X.; Zhu, T.; Wang, H.; Ye, D.; Hong, X. Removal of gas phase dimethylamine and *N,N*-dimethylformamide using non-thermal plasma. *Chem. Eng. J.* **2016**, *299*, 184–191. [CrossRef]

9. Xu, N.; Fu, W.; He, C.; Cao, L.; Liu, X.; Zhao, J.; Pan, H. Benzene removal using non-thermal plasma with CuO/AC catalyst: Reaction condition optimization and decomposition mechanism. *Plasma Chem. Plasma Process.* **2014**, *34*, 1387–1402. [CrossRef]

10. Feng, F.; Zheng, Y.; Shen, X.; Zheng, Q.; Dai, S.; Zhang, X.; Huang, Y.; Liu, Z.; Yan, K. Characteristics of back corona discharge in a honeycomb catalyst and its application for treatment of volatile organic compounds. *Environ. Sci. Technol.* **2015**, *49*, 6831–6837. [CrossRef] [PubMed]

11. Van Durme, J.; Dewulf, J.; Sysmans, W.; Leys, C.; Van Langenhove, H. Abatement and degradation pathways of toluene in indoor air by positive corona discharge. *Chemosphere* **2007**, *68*, 1821–1829. [CrossRef] [PubMed]

12. Vandenbroucke, A.M.; Morent, R.; De Geyter, N.; Leys, C. Non-thermal plasmas for non-catalytic and catalytic VOC abatement. *J. Hazard. Mater.* **2011**, *195*, 30–54. [CrossRef] [PubMed]

13. Satoh, K.; Matsuzawa, T.; Itoh, H. Decomposition of benzene in a corona discharge at atmospheric pressure. *Thin Solid Films* **2008**, *516*, 4423–4429. [CrossRef]

14. Schmid, S.; Jecklin, M.C.; Zenobi, R. Degradation of volatile organic compounds in a non-thermal plasma air purifier. *Chemosphere* **2010**, *79*, 124–130. [CrossRef] [PubMed]

15. Fan, X.; Zhu, T.L.; Wang, M.Y.; Li, X.M. Removal of low-concentration BTX in air using a combined plasma catalysis system. *Chemosphere* **2009**, *75*, 1301–1306. [CrossRef] [PubMed]

16. Hung Quang, T.; Mok, Y.S. Plasma-catalytic oxidation of acetone in annular porous monolithic ceramic-supported catalysts. *Chem. Eng. J.* **2014**, *251*, 199–206.

17. Zhu, X.; Tu, X.; Mei, D.; Zheng, C.; Zhou, J.; Gao, X.; Luo, Z.; Ni, M.; Cen, K. Investigation of hybrid plasma-catalytic removal of acetone over CuO/gamma-Al$_2$O$_3$ catalysts using response surface method. *Chemosphere* **2016**, *155*, 9–17. [CrossRef] [PubMed]

18. Narengerile; Watanabe, T. Acetone decomposition by water plasmas at atmospheric pressure. *Chem. Eng. Sci.* **2012**, *69*, 296–303.

19. Protection, T.C.M.O.E. *Emission Standard of Pollutants for Petroleum Chemistry Industry*; Chinese Environment Science Press: Beijing, China, 2015.

20. Ramaraju, B.; Karuppiah, J.; Linga Reddy, E.; Manoj Kumar Reddy, P.; Subrahmanyam, C. Removal of mixture of VOCs by nonthermal plasma. *Compos. Interfaces* **2012**, *19*, 271–277. [CrossRef]

21. Schiavon, M.; Scapinello, M.; Tosi, P.; Ragazzi, M.; Torretta, V.; Rada, E.C. Potential of non-thermal plasmas for helping the biodegradation of volatile organic compounds (VOCs) released by waste management plants. *J. Clean. Prod.* **2015**, *104*, 211–219. [CrossRef]

22. Zheng, C.; Zhu, X.; Gao, X.; Liu, L.; Chang, Q.; Luo, Z.; Cen, K. Experimental study of acetone removal by packed-bed dielectric barrier discharge reactor. *J. Ind. Eng. Chem.* **2014**, *20*, 2761–2768. [CrossRef]

23. Xia, D.; Li, Z.; Xie, Y.; Zhang, X. Kinetic simulations of volatile organic compounds decomposition by non-thermal plasma treatment. *Water Air Soil Pollut.* **2016**, *227*, 463. [CrossRef]

24. Alzueta, M.U.; Serinyel, Z.; Simmie, J.M.; Curran, H.J. Oxidation of acetone and its interaction with nitric oxide. *Energy Fuel.* **2010**, *24*, 1511–1520. [CrossRef]

25. Sun, W.; Uddi, M.; Won, S.H.; Ombrello, T.; Carter, C.; Ju, Y. Kinetic effects of non-equilibrium plasma-assisted methane oxidation on diffusion flame extinction limits. *Combust. Flame* **2012**, *159*, 221–229. [CrossRef]

26. Karatum, O.; Deshusses, M.A. A comparative study of dilute VOCs treatment in a non-thermal plasma reactor. *Chem. Eng. J.* **2016**, *294*, 308–315. [CrossRef]

27. Holzer, F.; Kopinke, F.D.; Roland, U. Influence of ferroelectric materials and catalysts on the performance of non-thermal plasma (NTP) for the removal of air pollutants. *Plasma Chem. Plasma Process.* **2005**, *25*, 595–611. [CrossRef]

28. Mallard, W.G.; Westley, F.; Herron, J.T.; Hampso, R. *NIST Chemical Kinetics Database: Version 2Q98*; NIST: Gaithersburg, MD, USA, 1998.

29. El-Maazawi, M.; Finken, A.N.; Nair, A.B.; Grassian, V.H. Adsorption and photocatalytic oxidation of acetone on TiO2: An in situ transmission FT-IR study. *J. Catal.* **2000**, *191*, 138–146. [CrossRef]

30. Barakat, C.; Gravejat, P.; Guaitella, O.; Thevenet, F.; Rousseau, A. Oxidation of isopropanol and acetone adsorbed on TiO_2 under plasma generated ozone flow: Gas phase and adsorbed species monitoring. *Appl. Catal. B* **2014**, *147*, 302–313. [CrossRef]

31. Bulanin, K.M.; Lavalley, J.C.; Tsyganenko, A.A. Infrared study of ozone adsorption on TiO_2 (Anatase). *J. Phys. Chem.* **1995**, *99*, 10294–10298. [CrossRef]

32. Xu, W.; Wang, N.; Chen, Y.; Chen, J.; Xu, X.; Yu, L.; Chen, L.; Wu, J.; Fu, M.; Zhu, A.; et al. In situ FT-IR study and evaluation of toluene abatement in different plasma catalytic systems over metal oxides loaded gamma-Al_2O_3. *Catal. Commun.* **2016**, *84*, 61–66. [CrossRef]

33. Evaluated Infrared Reference Spectra. *NIST Standard Reference Database*; National Institute of Standards and Technology: Gaithersburg, MD, USA, 2017.

34. Fan, X.; Zhu, T.; Wan, Y.; Yan, X. Effects of humidity on the plasma-catalytic removal of low-concentration BTX in air. *J. Hazard. Mater.* **2010**, *180*, 616–621. [CrossRef] [PubMed]

35. Yan, X.; Zhu, T.; Fan, X.; Sun, Y. Removal of p-chlorophenol in mist by DC corona discharge plasma. *Chem. Eng. J.* **2014**, *245*, 41–46. [CrossRef]

36. San, N.; Hatipoğlu, A.; Koçtürk, G.; Çınar, Z. Photocatalytic degradation of 4-nitrophenol in aqueous TiO_2 suspensions: Theoretical prediction of the intermediates. *J. Photochem. Photobiol. A* **2002**, *146*, 189–197. [CrossRef]

37. Bahri, M.; Haghighat, F.; Rohani, S.; Kazemian, H. Metal organic frameworks for gas-phase VOCs removal in a NTP-catalytic reactor. *Chem. Eng. J.* **2017**, *320*, 308–318. [CrossRef]

38. Sugasawa, M.; Terasawa, T.; Futamura, S. Additive Effect of Water on the Decomposition of VOCs in Nonthermal Plasma. *IEEE T. Ind. Appl.* **2010**, *46*, 1692–1698. [CrossRef]

39. Shahna, F.G.; Bahrami, A.; Alimohammadi, I.; Yarahmadi, R.; Jaleh, B.; Gandomi, M.; Ebrahimi, H.; Abedi, K.A.D. Chlorobenzene degeradation by non-thermal plasma combined with EG-TiO_2/ZnO as a photocatalyst: Effect of photocatalyst on CO_2 selectivity and byproducts reduction. *J. Hazard. Mater.* **2017**, *324*, 544–553. [CrossRef] [PubMed]

40. Lee, H.M.; Chang, M.B. Abatement of gas-phase p-xylene via dielectric barrier discharges. *Plasma Chem. Plasma Process.* **2003**, *23*, 541–558. [CrossRef]

41. Rosocha, L.A.; Korzekwa, R.A. Advanced oxidation and reduction processes in the gas phase using non-thermal plasmas. *J. Adv. Oxid. Technol.* **1999**, *4*, 247–264.

42. Andersen, K.B.; Beukes, J.A.; Feilberg, A. Non-thermal plasma for odour reduction from pig houses—A pilot scale investigation. *Chem. Eng. J.* **2013**, *223*, 638–646. [CrossRef]

43. Zhu, X.; Zhang, S.; Yang, Y.; Zheng, C.; Zhou, J.; Gao, X.; Tu, X. Enhanced performance for plasma-catalytic oxidation of ethyl acetate over La1-xCexCoO3 catalysts. *Appl. Catal. B* **2017**, *213*, 97–105. [CrossRef]

Sample Availability: Not available.